Scale Dependent Pomeron Intercept in Electromagnetic Diffractive Processes

H. G. Dosch
Institut für Theoretische Physik, Universität Heidelberg
Philosophenweg 16, D-69120 Heidelberg, Germany

E. Ferreira
Instituto de Física, Universidade Federal do Rio de Janeiro
C.P. 68528, Rio de Janeiro 21945-970, RJ, Brazil

We test the hypothesis that diffractive scattering in the perturbative and non-perturbative domain is determined by the exchange of a single pomeron with a scale dependent trajectory. Present data on diffractive vector meson production are well compatible with this model and recent results for J/ψ photoproduction at LHC strongly support it. The model is inspired by concepts of gauge/string duality applied to the pomeron.

I. INTRODUCTION

Diffractive processes involving virtual photons show a remarkable feature: the higher the photon virtuality Q^2, the faster is the increase of the cross sections with energy. This feature is well understood in perturbative QCD, where the evolution equations in Q^2 [1–3] predict such behaviour. Microscopically, the rising increase in energy can be traced back to the increase of the gluon density with higher resolution. This specific feature of the energy dependence, however, is less easily explained in Regge theory. In purely hadronic diffractive processes the energy dependence of the scattering amplitude is determined by the pomeron trajectory to be $W^{2\alpha_P(t)}$ where W is the cm energy, $\alpha_P(t) = \alpha_P(0) + \alpha'_P t$ is the pomeron trajectory, and t is the squared momentum transfer. Based on a large amount of hadronic diffractive data, Donnachie and Landshoff [4] proposed a general description with a hypercritical pomeron intercept $\alpha_P(0) \approx 1.09$ and a slope $\alpha'_P = 0.25\,\mathrm{GeV}^{-2}$.

Electroproduction processes can be related to purely hadronic interactions through the assumption that the photon-hadron interaction occurs via the interaction of the target hadron with a quark-antiquark pair, as illustrated in Fig.1. According to this model, diffractive electromagnetic processes are described as purely hadronic processes, with energy dependence governed by the pomeron trajectory. This approach, commonly called dipole picture [5], has been tested in many analyses and applications. Although there are certain limitations to this approach [6, 7] it is intuitive and phenomenologically very successful.

On the other hand, by summing up leading log terms in perturbative QCD, a larger pomeron intercept was found (BFKL-Pomeron) [8–12]. Donnachie and Landshoff [13] extended the pomeron concept and assumed that electromagnetic diffractive processes are determined by two pomerons, a soft (hypercritical) one with an intercept of about 1.09 and a hard one with an intercept of about 1.4. This idea has been applied in many electroproduction processes, where the residues of the pomerons were essentially determined by the size of the scattered objects
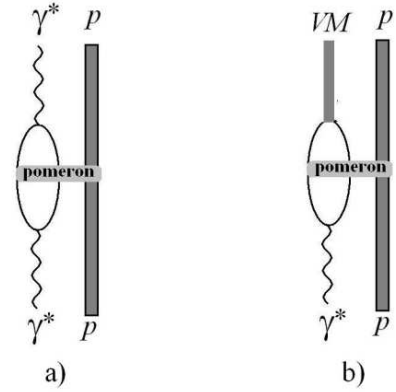

FIG. 1. Electromagnetic diffractive processes in the dipole model governed by pomeron exchange: a) γ^* scattering; b) electroproduction of vector mesons (VM) .

and hence in a given model the energy dependence was universally fixed by a superposition of the two pomeron contributions. In this way a comprehensive description of proton structure functions, vector meson production and $\gamma^* - \gamma^*$ scattering could be achieved in the full energy range accessible at HERA [14–21].

Recent experiments on J/ψ photoproduction at LHC energies [22, 23], however, show that a single power, corresponding to a pomeron intercept at about 1.17, describes very well the energy dependence in the range from 20 GeV to 1 TeV. This result strongly supports the concept of a single pomeron exchange.

The AdS/CFT correspondence [24–26] has opened interesting new aspects to pomeron physics [27, 28]. In a very simple model in an ultralocal approximation, discussed at the beginning of [27] it was shown that the pomeron trajectory depends on the holographic variable z

$$\alpha_P(t, z) = \alpha_P(0) + \alpha'_P(z)\, t \,, \tag{1}$$

with

$$\alpha'_P(z) = \alpha' \frac{z^2}{R^2} \ , \qquad (2)$$

where α' is a constant relevant for scattering of the strings in the higher dimensional space and R is the AdS scale. The holographic variable z used here is related to the r in [27] by $z = R^2/r$. In this simple model the intercept value is $\alpha_P(0) = 2$ [29].

With the assumption of a single pomeron the value of the intercept should be nearly one in order to describe purely hadronic diffraction processes, whereas experimentally it is distinctly larger for diffractive processes with high photon virtuality. Therefore, in a bottom-up approach to the problem, we are led to extend the concept of a scale dependent pomeron slope, Eq.(2), to that of a scale dependent intercept, $\alpha_P(0, z)$. In order to test this assumption quantitatively, we use in the present work a phenomenologically very successful approach to AdS/CFT duality, namely light front holographic QCD, developed by de Téramond and Brodsky [31] (for a review see [32]). One essential point is the discovery that the AdS bound state equations are identical with the light front (LF) bound state equations, if one identifies the holographic variable z with the boost invariant light-front separation ζ between the quark and the antiquark inside a hadron (details are given in the next section). It has been shown that the bound state wave functions obtained in light-front holographic QCD give a very good fit to rho-meson electroproduction [33], and it was shown [20] that the light-front wave functions [34] are indeed very appropriate for the description of electroproduction not only of ρ mesons, but also of other vector mesons as J/ψ and Υ. In the present work we use the coincidence of the holographic variable z with the boost invariant light front separation ζ in order to determine the scale, on which the pomeron intercept is assumed to depend, for different diffractive processes. We proceed in the following way. First the scale for different processes is determined and then the dependence of the pomeron intercept is extracted from an analysis of the energy dependence of the structure functions [35, 36] on the scale. This intercept determines the energy behaviour of all processes with the same scale, and the energy dependence of different processes, as $\gamma^* p$ scattering and vector meson electroproduction, can be related.

Our paper is organized as follows: In Sect.II we determine the scale for the different processes and give interpolation formulæ which relate the scale to the photon virtuality; in Sect.III the pomeron intercept as function of the scale and the photon virtuality is derived from the energy dependence of the structure functions. In Sect.IV we present comparison with experiments and finally we summarize and discuss our results in Sect.V.

II. FIXING THE SCALE FOR DIFFERENT PROCESSES

Vector meson production and $\gamma^* p$ scattering are the best investigated electromagnetic diffractive processes. In the dipole model, for a fixed cm energy $W_0 = \sqrt{s_0}$, of the γ^* and the target the forward scattering amplitude is generically given by [5]

$$\mathcal{T}_0 = i \int_0^\infty d\zeta \int_0^1 du \frac{\zeta}{u\bar{u}} \ \sigma(u, \zeta) \ \rho(Q^2, u, \zeta) \ , \qquad (3)$$

where u and $\bar{u} = 1 - u$ are the longitudinal momentum fractions of the dipole constituents, and

$$\zeta = \sqrt{u\,\bar{u}} \ r_\perp \ , \qquad (4)$$

$r_\perp$ being their transverse separation.

The quantity $\sigma(u, \zeta)$ is the dipole cross section and $\rho(Q^2, u, \zeta)$ the overlap of the wave functions of the virtual photon and of the diffractively produced particle. Eq. 3 determines the Regge residue and the energy dependence of the forward amplitude in the Regge model is $\mathcal{T} = \mathcal{T}_0 (s/s_0)^{\alpha_P}$.

The overlap, written generically as

$$\rho_{\gamma^*, fs}(Q^2, u, \zeta) = \psi_{fs}^*(u, \zeta) \ \psi_{\gamma^*}(Q^2, u, \zeta), \qquad (5)$$

is represented diagrammatically in Fig.1. Here $\psi_{\gamma^*}(Q^2, u, \zeta)$ is the hadronic wave function of the incident photon, and $\psi_{fs}(u, \zeta)$ is the wave function of the final state; for vector meson production it is the vector meson wave function, while for γ^* scattering it is the outgoing hadronic photon wave function.

For the overlap functions we present below the simple and phenomenologically successful forms, which at fixed cm energy W describe very satisfactorily the Q^2 dependence of the different processes [16, 18, 19, 21]. Conservation of s-channel helicity is assumed [37].

For $\gamma^* p$ scattering with transverse polarization we write

$$\rho_{\gamma^* \gamma^* \pm 1}(Q^2, u, \zeta) = \hat{e}_f^2 \frac{6\alpha}{4\pi^2} \qquad (6)$$
$$\left[(Q^2 \, u(1 - u) + m_f^2)(u^2 + (1 - u)^2) \, K_1^2(\hat{\epsilon}\zeta) + m_f^2 \, K_0^2(\hat{\epsilon}\zeta) \right]$$

and for longitudinal polarization

$$\rho_{\gamma^* \gamma^* 0}(Q^2, u, \zeta) \qquad (7)$$
$$= \hat{e}_f^2 \frac{12\alpha}{4\pi^2} \ Q^2 \, u^2 (1 - u)^2 \, K_0^2(\hat{\epsilon}\zeta) \ ,$$

where

$$\hat{\epsilon} = \sqrt{Q^2 + \frac{m_f^2}{u(1 - u)}} \ , \qquad (8)$$

and with m_f representing the mass of the quarks forming the dipole in the LHS of Fig. 1.

The overlap functions connecting γ^* and vector mesons are for transverse polarization

$$\rho_{\gamma^*,V;\pm 1}(Q^2,u,\zeta) = \hat{e}_V \frac{\sqrt{6\alpha}}{2\pi} \tag{9}$$
$$\left[4\hat{\epsilon}\,\zeta\,\omega^2(u^2+(1-u)^2)\,K_1(\hat{\epsilon}\zeta) + m_f^2\,K_0(\hat{\epsilon}\zeta)\right]\phi_\omega(u,\zeta)\,,$$

and for longitudinal polarization

$$\rho_{\gamma^*,V;0}(Q^2,u,\zeta) \tag{10}$$
$$= 16\hat{e}_V \frac{\sqrt{3\alpha}}{2\pi}\,\omega\,Q\,u^2(1-u)^2\,K_0(\hat{\epsilon}\zeta)\,\phi_\omega(u,\zeta)\,,$$

with mass m_f for the quarks constituting the vector meson. $\phi_\omega(u,\zeta)$ is the Brodsky-Lepage (BL) [34] wave function parameter ω, written

$$\phi_\omega(u,\zeta) = \frac{N}{\sqrt{4\pi}}\exp\left[-\frac{m_f^2(u-1/2)^2}{2u(1-u)\omega^2}\right]\exp[-2\omega^2\zeta^2]\,. \tag{11}$$

(In the wave functions derived from light front holographic QCD [31] an additional factor $\sqrt{u(1-u)}$ appears; the influence of this factor, however, on the value of the scale is negligible). For convenience, the values of ω in the BL wave function (11), determined by the electronic decay widths [20, 21] are given in Table I.

Our final results do not depend strongly on the form of the dipole cross section, since it enters into the calculation for photon scattering and vector-meson production in the same way. The simplest choice is the quadratic form

$$\sigma(u,\zeta) = c\,r_\perp^2 = c\,\frac{\zeta^2}{u\bar{u}}\,. \tag{12}$$

We also use a form obtained directly from the data by a deconvolution of experimental data [38, 39]. This dipole cross section starts to grow with the third power of $r_\perp$ and decreases for $r_\perp > 3$ GeV^{-1}, as shown in Fig.2. The value of the scale does not depend on the magnitude of the dipole cross section but only on its form. In the following we shall use the quadratic form, unless stated explicitly.

In order to extract a fixed representative scale $\bar{\zeta}$ for a specific process and a given Q^2 value, we determine the ζ value where the overlap is maximal, namely find $\bar{\zeta}_{\max}$ that gives the maximum of the integrand Y in Eq.(3)

$$Y(Q^2,\zeta) = \int_0^1 du\,\frac{\zeta}{u\bar{u}}\sigma(u,\zeta)\,\rho(Q^2,u,\zeta)\,. \tag{13}$$

Typical forms of the function $Y(Q^2,\zeta)$ for two chosen processes with the quadratic dipole cross section and selected Q^2 values are shown in Fig.3. As we are interested in showing that both overlap functions have marked maxima positions, but different shapes, the curves are presented normalized to 1 at the peak, and two Q^2 values are chosen that show peaks at the same value of $\bar{\zeta}_{\max}$. The values represented in the figure are $Q^2 = 1.5$ GeV^2 for $\rho_{\gamma^*,\gamma^*,1}$ and $Q^2 = 26$ GeV^2 for $\rho_{\gamma^*\rho,1}$.
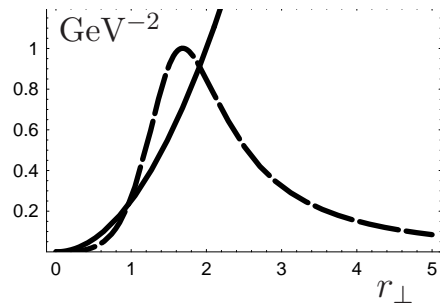

FIG. 2. Dipole cross sections. The solid line represents the usual quadratic form (12), and the dashed line plots the form given in [38].
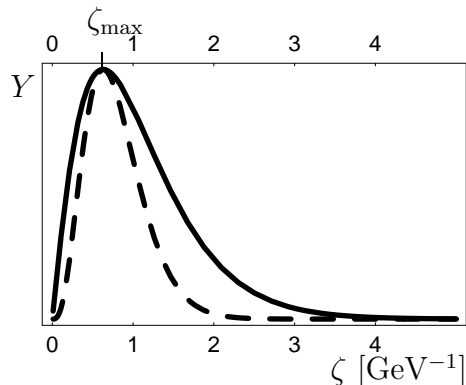

FIG. 3. The function Y, Eq. (13), for $\rho_{\gamma^*,\gamma^*,1}$ at $Q^2 = 1.5$ GeV^2 (solid curve) and for $\rho_{\gamma^*\rho,1}$ at $Q^2 = 26$ GeV^2 (dashed curve) for the quadratic dipole cross section (12) as function of ζ. The displayed Q^2 values are chosen to yield the same $\bar{\zeta}_{\max}$ values, and the curves are normalized to equal height at $\bar{\zeta}_{\max}$.

In order to obtain some control of the uncertainties of this choice of a representative scale, we also use another intuitive criterion. We define $\bar{\zeta}_{\mathrm{med}}$ as the median value of ζ, determined by

$$\int_0^{\bar{\zeta}_{\mathrm{med}}} d\zeta \int_0^1 du\,\frac{\zeta}{u\bar{u}}\sigma(u,\zeta)\rho(Q^2,u,\zeta) \tag{14}$$
$$= \int_{\bar{\zeta}_{\mathrm{med}}}^\infty d\zeta \int_0^1 du\frac{\zeta}{u\bar{u}}\sigma(u,\zeta)\rho(Q^2,u,\zeta)\,.$$

The cross sections of longitudinal and transverse photons are added incoherently, and we therefore have fitted independently the scales for both polarizations and for their weighted average, for the different processes and interesting Q^2 values.

The overlap functions $\rho(Q^2,u,\zeta)$ depend on the quark masses. For diffractive production of heavy vector mesons we use the $\overline{MS}$ masses [40]: $m_c = 1.28$ GeV
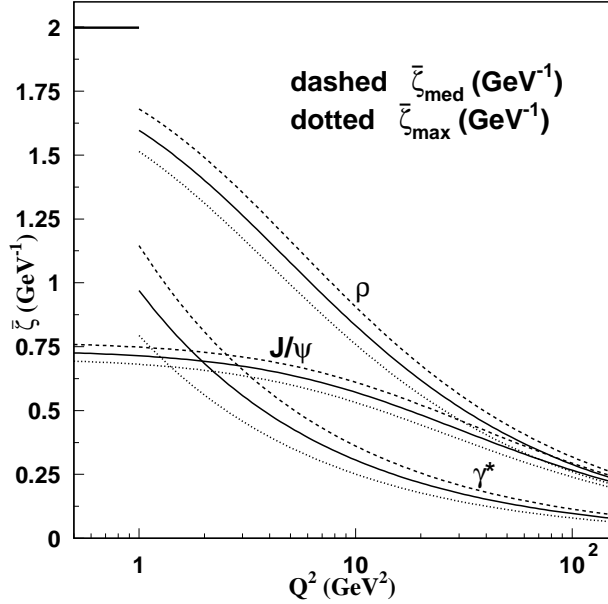
FIG. 4. Plots of functions $\bar{\zeta}_{\max}(Q^2)$ and $\bar{\zeta}_{\mathrm{med}}(Q^2)$ that convert Q^2 into the scale variables that are used to describe different diffractive processes of ρ and J/ψ vector meson production and photon scattering. The solid line represents their average $\bar{\zeta}$ given in Eq.20.

and $m_b = 4.18$ GeV. For $Q^2 = 0$ the overlap diverges logarithmically with vanishing quark mass and therefore special constituent mass values have to be assumed. In order to reduce model dependence, we have for light meson production determined the scale only for $Q^2 \geq 1$, where the dependence on quark masses is weak and the current quark masses, $m_u \approx m_d \approx 0$, $m_s = 0.1$ GeV can safely be chosen. For hadronic processes involving light quarks, the scale at $Q^2 = 0$ is fixed by the confinement scale and therefore we have there the purely hadronic pomeron intercept $\alpha_{\mathbf{P}} \approx 1.09$.

Fig.4 shows the functions $\bar{\zeta}_{\max}(Q^2)$ and $\bar{\zeta}_{\mathrm{med}}(Q^2)$ and their average $\bar{\zeta}(Q^2)$ for ρ and J/ψ vector meson production and for photon scattering.

| | Transverse | | Longitudinal | |
| | ω | N | ω | N |
	(GeV)		(GeV)	
$\rho(770)$	0.2809	2.0820	0.3500	1.8366
$\omega(782)$	0.2618	2.0470	0.3088	1.8605
$\phi(1020)$	0.3119	1.9201	0.3654	1.9191
$J/\psi(1S)$	0.6452	1.4752	0.7140	2.2769
$\Upsilon(1S)$	1.3333	1.1816	1.3851	2.7694

TABLE I. Parameters of the Brodsky-Lepage (BL) vector meson wave functions (11), taken from [20, 21].

III. SCALE DEPENDENT POMERON INTERCEPT

The best investigated electromagnetic diffractive process is $\gamma^* p$ scattering. It is usually presented as the DIS proton structure function $F_2(x, Q^2)$, which is related to the $\gamma^* p$ total cross section by

$$F_2(x, Q^2) = \frac{Q^2}{4\pi^2\,\alpha}\sigma^{\gamma^* p} \ , \qquad (15)$$

with

$$x = \frac{Q^2}{W^2 + Q^2 - m_p^2} \ . \qquad (16)$$

Due to the optical theorem the total $\gamma^* p$ cross section is proportional to the $\gamma^* p$ forward scattering amplitude and its energy behaviour is given by the pomeron intercept at $t = 0$, with the form $W^{2[\alpha_{\mathrm{P}}(0)-1]}$.

The structure function has been fitted [41] with the power behaviour

$$F_2(x, Q^2) = c\ Q^2\ x^{-\lambda(Q^2)} \ , \qquad (17)$$

with $\lambda(Q^2) = 0.0481 \log\left[Q^2/0.0853\right]$ for $Q^2 \geq 3.5$ GeV^2, related to the pomeron intercept by $\lambda = \alpha_{\mathbf{P}}(0) - 1$. We use the modification

$$\alpha_{\mathbf{P}}(0) - 1 = 0.0481 \log\left[\frac{Q^2 + 0.554}{0.0853}\right] \ , \qquad (18)$$

that is adjusted to give the intercept 1.09 at hadronic scales, that is at $Q^2 = 0$.

In order to relate the pomeron intercept with the scale $\bar{\zeta}$ one inverts the scale function $\bar{\zeta}_\gamma(Q^2)$, obtained for $\gamma^* p$ scattering according to the methods explained in the preceding section; this yields the inverse function $\overline{Q^2}_\gamma(\bar{\zeta})$. One can then calculate the value of the intercept of vector meson production as function of Q^2 from (18) by inserting for Q^2 the value $\overline{Q^2}(\bar{\zeta}_{VM})$, where $\bar{\zeta}_{VM}$ is the value $\bar{\zeta}_{\mathrm{VM}}(Q^2)$ obtained for the vector meson at photon virtuality Q^2. We thus obtain for the production of the vector meson VM the relation

$$\alpha_{\mathbf{P}}(0) - 1 = 0.0481 \log\left[\frac{\overline{Q^2}_\gamma\big(\bar{\zeta}_{\mathrm{VM}}(Q^2)\big) + 0.554}{0.0853}\right] \ . \ (19)$$

It turns out that the intercept calculated for a specific process at fixed Q^2 depends only weakly on the method of its extraction, the deviation of $\alpha_P(0) - 1$ obtained for both procedures $\bar{\zeta}_{\max}$ and $\bar{\zeta}_{\mathrm{med}}$ deviates at most $\pm 5\%$ from the mean value $\bar{\zeta}$. We therefore present in the following only the averaged results

$$\bar{\zeta}(Q^2) = \frac{1}{2}[\bar{\zeta}_{\max}(Q^2) + \bar{\zeta}_{\mathrm{med}}(Q^2)] \ . \qquad (20)$$

The extreme choice of the dipole cross section of [38] leads to an increase of $\alpha_P(0) - 1$ by less than 15 %.

The results of the numerical analysis show that for each process $\gamma^* p \to fs\, p$ with final state fs and given polarization "pol", the average scale $\bar{\zeta}(Q^2)$ can be very well fitted by a function of the simple form

$$\bar{\zeta}_{fs}(Q^2) = \frac{a_{fs,pol}}{\sqrt{Q^2 + b_{fs,pol}}} \ . \tag{21}$$

The coefficients a and b for the different processes are displayed in Table II.

From this fit and Eq.(19) we can obtain the pomeron intercept from γ^* scattering as a function of the scale $\bar{\zeta}$. We then have

$$\alpha_{\mathbf{P}}(0) - 1 = 0.0481 \log \left[\frac{a_{\gamma^*,\mathrm{pol}}^2 / \bar{\zeta}^2 - b_{\gamma^*,\mathrm{pol}} + 0.554}{0.0853} \right] , \tag{22}$$

where $a_{\gamma^*,\mathrm{pol}}$ is the coefficient in Eq.(21) for $\gamma^* p$ scattering, with the label pol indicating transverse (T), longitudinal(L) or total (tot) cross sections (row γ^* in Table II).

From this equation we obtain the intercept for vector meson production as function of Q^2 by expressing the scale $\bar{\zeta}$ through Eq.(21) for the specified meson VM

$$\delta(Q^2) = 4(\alpha_{\mathbf{P}}(0) - 1) = 0.472 + 0.1924 \times \tag{23}$$

$$\log \left[\frac{a_{\gamma^*,\mathrm{pol}}^2}{a_{\mathrm{VM,pol}}^2} (Q^2 - b_{\gamma^*,\mathrm{pol}} + b_{\mathrm{VM,pol}}) + 0.554 \right] \ .$$

final state	$a_{fs,\mathrm{pol}}$			$b_{fs,\mathrm{pol}}$ [GeV^2]		
fs	trans	long	total	trans	long	total
γ^*	0.945	1.228	0.968	-0.004	-0.003	-0.004
ρ	3.602	2.767	2.925	2.724	2.092	2.357
ϕ	3.651	2.800	3.022	3.308	2.581	2.351
J/ψ	3.386	2.790	2.856	20.63	17.12	14.98
Υ	3.186	2.765	2.658	123.2	109.6	86.93

TABLE II. Coefficients of the numerical fits of the average scale $\bar{\zeta}_{fs}(Q^2)$, (20), for the processes $\gamma^* p \to fs\, p$ with Eq.(21), for use in longitudinal, transverse and total (incoherent sum of the two cases) cross sections. $fs = \gamma^*$ refers to γ^*p total cross section. The accuracy of the fit is better than 1% in the Q^2 range from 1 to 60 GeV^2 for photon scattering and ρ, ϕ production and from 0 to 60 GeV^2 for J/ψ and Υ production. Remark: For $Q^2 = 0$ in ρ and ϕ production, the relevant scale is the hadronic scale, chosen as $\bar{\zeta} = 2\,\mathrm{GeV}^{-1}$, with a soft pomeron intercept 1.09.

The intercept at $t = 0$ determines the energy behaviour of the forward scattering amplitude (and therefore also of the total $\gamma^* p$ cross section). For integrated elastic production cross sections one also has to take into account the t dependence of the trajectory, which leads to a shrinkage of the diffraction peak. For unpolarized elastic diffractive vector meson production, $\gamma^* p \to p\,[\mathrm{VM}]$, the differential elastic cross section in the Regge model is given by

$$\frac{d\sigma}{dt} = \left(\frac{s}{s_0} \right)^{2[\alpha_{\mathbf{P}}(t)-1]} \beta^2(t) \ . \tag{24}$$

For fixed W and Q^2 the t dependence is well approximated by an exponential, and we thus assume the residue $\beta(t) = \beta_0 e^{Bt/2}$ and $\alpha_{\mathbf{P}}(t) = \alpha_{\mathbf{P}}(0) + \alpha'_{\mathbf{P}} t$. We then obtain for the integrated cross section

$$\sigma_{\mathrm{int}} = \int_{-\infty}^{0} dt \, \frac{d\sigma}{dt} \tag{25}$$

$$= \frac{\beta_0^2}{B + 2\alpha'_{\mathbf{P}} \log(s/s_0)} \left(\frac{s}{s_0} \right)^{2[\alpha_{\mathbf{P}}(0)-1]} \left(1 + O(s^{-2}) \right) \ .$$

The slopes observed in $d\sigma/dt$ in vector meson electroproduction [20] are in the range of 5 to 10 GeV^{-2}. With $2\alpha'_{\mathbf{P}}/B \ll 1$, the energy dependence of the total cross section can be approximated by

$$\sigma_{\mathrm{int}} \approx \frac{\beta_0^2}{B} \left(\frac{s}{s_0} \right)^{2[\alpha_{\mathbf{P}}(0)-\alpha'_{\mathbf{P}}/B-1]} \ . \tag{26}$$

Although the present data on $\alpha'_{\mathbf{P}}$ do not allow firm conclusions [36], it is certain that the effective powers δ_{VM} that fits experiments should be smaller than the value $4[\alpha_{\mathbf{P}}(0)-1]$ obtained from the structure function. In the simplified model of Eq.(2) [27] discussed in the introduction, the slope of the pomeron trajectory decreases with decreasing scale

$$\alpha'_{\mathbf{P}} = \alpha' \frac{\bar{\zeta}^2}{\bar{\zeta}_{\mathrm{conf}}^2} \ , \tag{27}$$

where $\bar{\zeta}_{\mathrm{conf}}$ is the scale set by confinement, at which $\alpha'_{\mathbf{P}} \approx 0.25$ GeV^{-2}. Choosing realistic values $\bar{\zeta}_{\mathrm{conf}} = 2$ GeV^{-1}, $B = 5$ GeV^{-2} we obtain a shrinking correction

$$\frac{\alpha'_{\mathbf{P}}}{B} = 0.0125\, \bar{\zeta}^2 = 0.0125 \frac{a_{\mathrm{VM,pol}}^2}{Q^2 + b_{\mathrm{VM,pol}}} \ , \tag{28}$$

and for the power δ_{int}, applicable to integrated elastic diffractive cross sections we have

$$\delta_{\mathrm{int}}(Q^2) = \delta - 4\alpha'_{\mathbf{P}}/B = 0.472 \tag{29}$$

$$+ 0.1924 \log \left[\frac{a_{\gamma^*,\mathrm{pol}}^2}{a_{\mathrm{VM,pol}}^2} (Q^2 - b_{\gamma^*,\mathrm{pol}} + b_{\mathrm{VM,pol}}) + 0.554 \right]$$

$$- 0.05 \frac{a_{\mathrm{VM,pol}}^2}{Q^2 + b_{\mathrm{VM,pol}}} \ .$$

IV. DESCRIPTION AND PREDICTION OF DIFFRACTIVE DATA

In Fig.5 experimentally determined values of the power $\delta = 4\left(\alpha_{\mathbf{P}}(0) - 1\right)$ for different reactions are displayed against the scale $\bar{\zeta}$. The values for photon scattering are deduced from measurements of the proton structure function and the total $\gamma^* p$ cross section [41, 42]. The experimental δ values for vector meson production are taken from: a) ρ-production [36, 43–46]; b) ϕ-production [36, 47]; c) J/ψ-production [48, 50, 51, 57]; d)
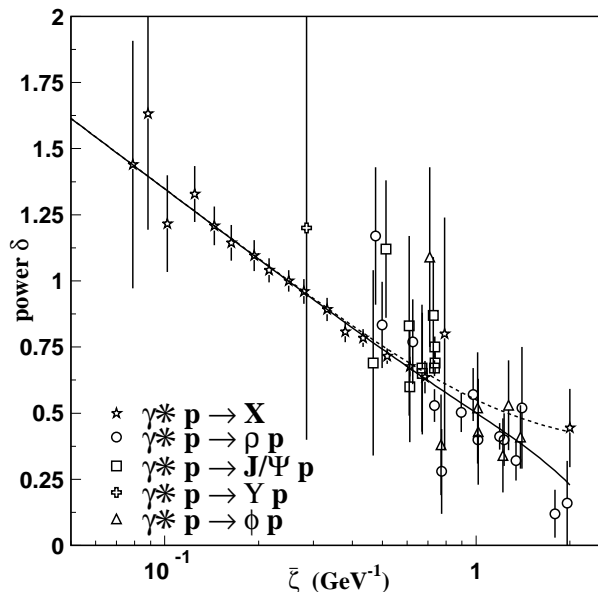
FIG. 5. Experimental values of $\delta = 4(\alpha_{\mathbf{P}}(0) - 1)$ vs. the scale $\bar{\zeta}$ for different processes. The dashed line represents the interpolation formula (18). The solid curve takes into account the effects of the shrinking in Eq.(27). The stars are obtained from measurements of the proton structure function and total $\gamma^* p$ cross section [41, 42]. References for the data on vector meson production are given in detail in Fig.6.

Υ-production [52]. They are given for fixed Q^2, and the corresponding scale $\bar{\zeta}$ has been determined by Eq.(21) with the constants from Table II. The dashed line corresponds to the fit Eq.(18) to the photon data with $Q^2 = 0.968^2/\bar{\zeta}^2 + 0.004$. The solid line includes the shrinkage correction Eq.(27),(28),(29) to be applied for the integrated cross sections of diffractive vector meson production.

The errors for vector meson production and correspondingly the fluctuations are generally quite large, but the figure shows that the data are well compatible with a common power behaviour, only dependent on the $\bar{\zeta}$ scale, but not on the process. Future data in the TeV region with reduced errors may provide decisive tests for the conjecture of a single pomeron with a scale dependent intercept governing the energy behaviour universally for all diffractive processes.

In Fig.6 we show theoretical predictions and experimental results for the powers δ and δ_{int}, that is without and with shrinkage correction, as a function of the photon virtuality Q^2 for unpolarized elastic production of all vector mesons in the ground state, the theoretical results for ω meson production are not distinguishable from those of ρ production. The long-dashed curves represent the uncorrected power $\delta(Q^2)$, obtained from Eq.(23), and the solid line is δ_{int}, Eq.(29) that includes shrinkage corrections. We also show with dotted lines results based on a scale determination with the rather extreme dipole cross

section [38] shown in Fig.2. The theoretical predictions are well compatible with the experiments. The observed sharp increase of the power delta with Q^2 near $Q^2 = 0$ indicates that the rapidly varying shrinkage correction given by Eq.(28) is quite realistic.

In in Fig.7 data and the theoretically predicted energy dependence of ρ and J/ψ cross section are displayed. According to the model the energy dependence is represented by a single power $c W^\eta$ in the full energy range . The constant c is fitted to the data, and the values for the power η are given by the model, either $\eta = \delta(Q^2)$ or $\eta = \delta_{\mathrm{int}}(Q^2)$. For ρ production (left hand side) we show both the results with shrinkage correction, Eq.(29), in solid lines, and without shrinkage correction, Eq.(23), in dashed lines. At $Q^2 = 0$ we have used $\delta(0) = 0.36$ corresponding to the soft pomeron intercept 1.09. The shrinkage correction reduces this vcalue to $\delta_{\mathrm{int}} = 0.18$. The data are clearly compatible with experiment, and it is expected that further data at LHC energies will be bring decisive test for the single power behaviour.

The plot of J/ψ photoproduction on the right hand side includes the most recent LHC data. Here the influence of the shrinking correction is small and $\delta(0) = 0.63$, $\delta_{\mathrm{shrink}}(0) = 0.61$ (solid line). To exhibit the stability of the predictions of the universality conjecture, the dotted line gives the prediction from the extreme dipole model of [38], displayed in Fig. 2.

Parameters of the curves $C W^\eta$ for J/ψ photoproduction in some cases are as follows:

theory with shrinkage correction Eq.(29): $\eta = \delta_{\mathrm{int}}(0) = 0.61$, $C = 4.99$, $\chi^2 = 1.35$;

theory without shrinkage correction (23): $\eta = \delta(0) = 0.63$, $C = 4.46$, $\chi^2 = 1.042$;

theory with dipole model of [38] without shrinkage correction: $\eta = \delta_{\mathrm{int}}(0) = 0.69$, $C = 3.37$, $\chi^2 = 0.84$;

free fit with open power: $\eta = 0.68$, $C = 3.61$, $\chi^2 = 0.81$.

The transverse and longitudinal wave functions are different and therefore we obtain different scales for the respective cross sections. This leads to different energy behaviour for the two polarizations and the ratio $R = \sigma_L/\sigma_T$ has the power behaviour

$$R = \frac{\sigma_L}{\sigma_T} = A W^{\delta_{\mathrm{R}}} , \qquad (30)$$

with

$$\delta_R = \delta_L - \delta_T . \qquad (31)$$

The values of δ_L and δ_T are determined by Eq.(23) with the constants $a_{\mathrm{VM,long}}$, $a_{\mathrm{VM,trans}}$, $b_{\mathrm{VM,long}}$, $b_{\mathrm{VM,trans}}$ of Table II. The experimental errors for the ratio R are quite large and also the theoretical uncertainties in the small differences between δ_L and δ_T are large.

In Fig. 8 a) - c) we show data [36, 45, 58] for the energy dependence of the polarization ratios $R = \sigma_L/\sigma_T$ for three values of Q^2. The solid line are the theoretical predictions according to Eqs. 23,30,31. The multiplicative constant A in Eq. (30) is fitted freely. We also show
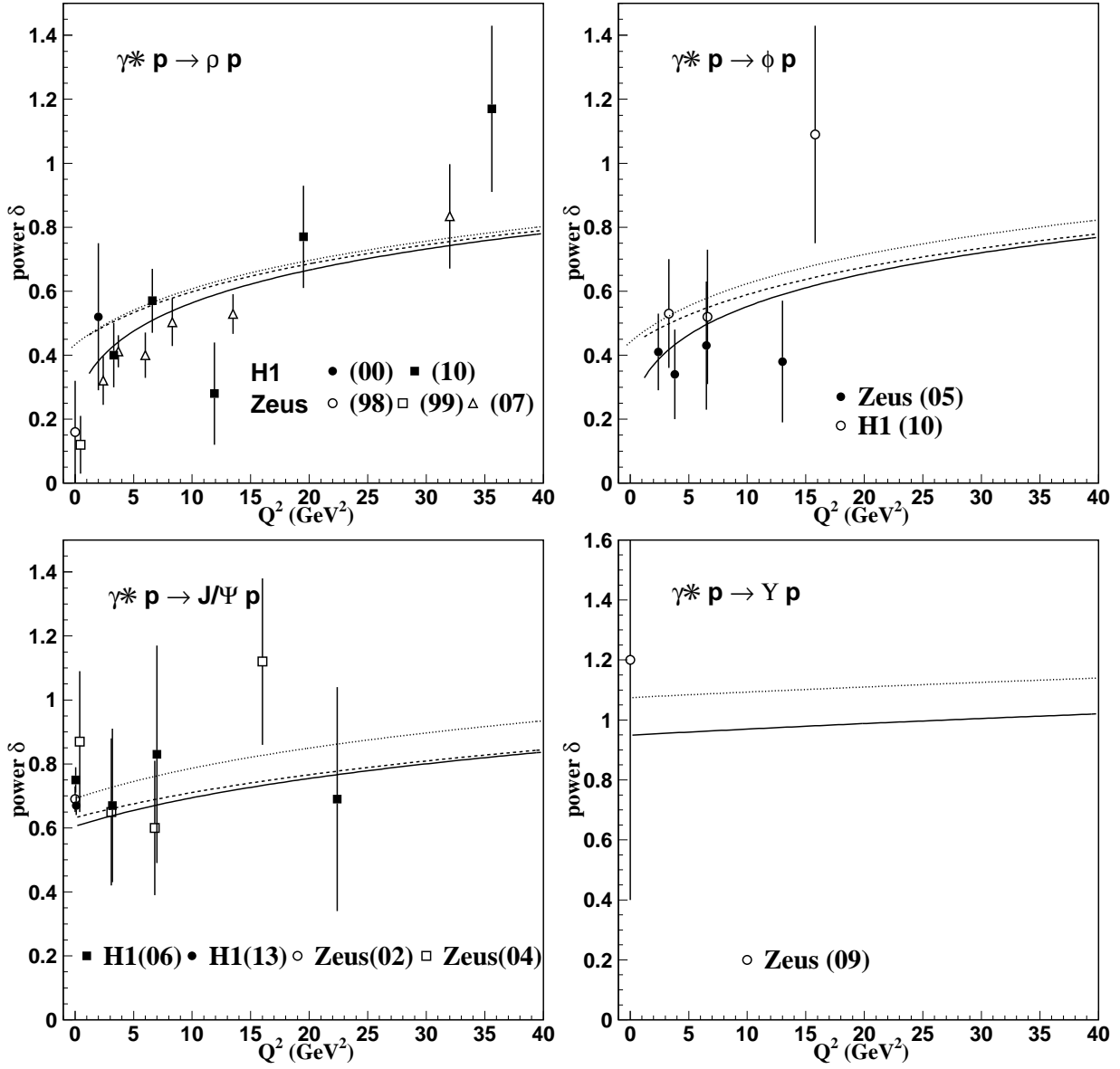
FIG. 6. Predictions for the power δ and δ_{int} as function of Q^2 for vector meson electroproduction and experimental values for this quantity: a) ρ-production [36, 43–46]; b) ϕ-production [36, 47] ; c) J/ψ-production [48, 50, 51, 57]; d) Υ-production [52]. The solid line is δ_{int}, Eq.(29), including the shrinkage correction, and the dashed line is δ, Eq. (23), as obtained with the quadratic dipole cross section. The power δ for the special dipole model [38] shown in Fig.2 is represented by the dotted line, without shrinkage corrections.

in dashed lines the results of free fits to the data with unconstrained A and δ_R. At $Q^2 = 7.5$ and 22.5 GeV^2 the model gives good agreement for the energy dependence of the ratio R. In the last plot of the set, the data and the theoretical predictions for the power coefficients as functions of Q^2 are compared directly.
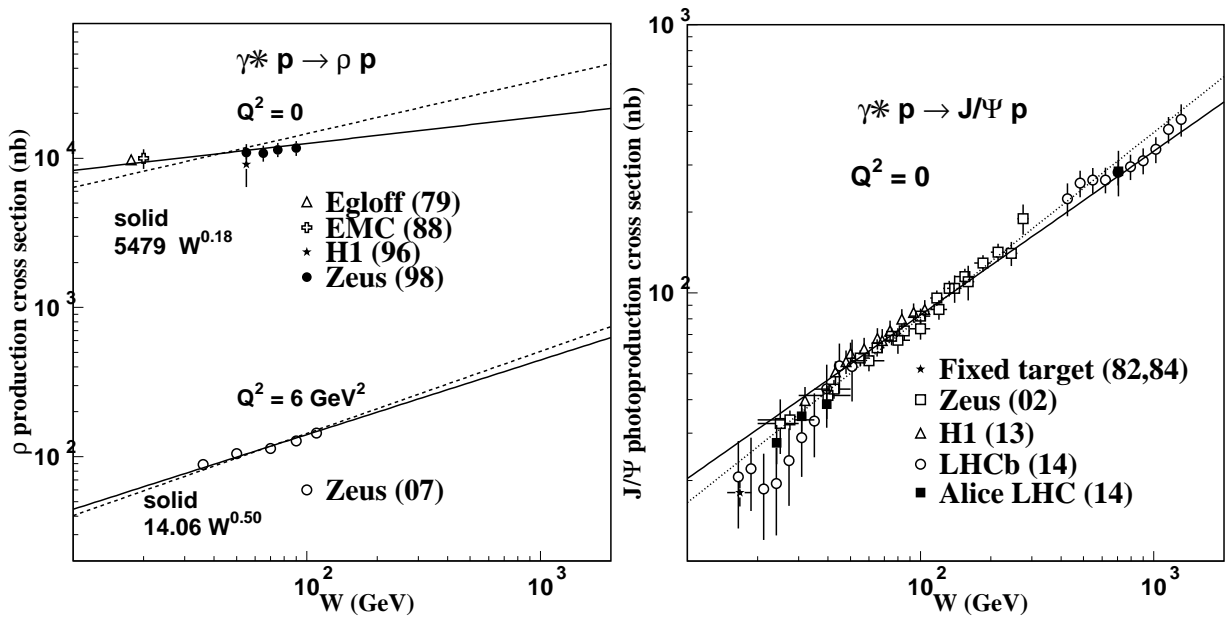
FIG. 7. Energy dependence of the integrated elastic cross sections for ρ and J/ψ production. For ρ production the dashed line shows the power behaviour without shrinkage correction, which is included in Eq.(29), represented by solid lines. For J/ψ production the solid line shows the behaviour with $\delta = 0.61$ including the (rather small) shrinkage correction, while the dotted line is from the extreme dipole cross section of [38] without shrinkage, with $\delta = 0.69$. The data for ρ production are from [43, 53–55] for $Q^2 = 0$, and from [45] for $Q^2 = 6$. For J/ψ photoproduction the data are from [22, 23, 50, 56, 57].
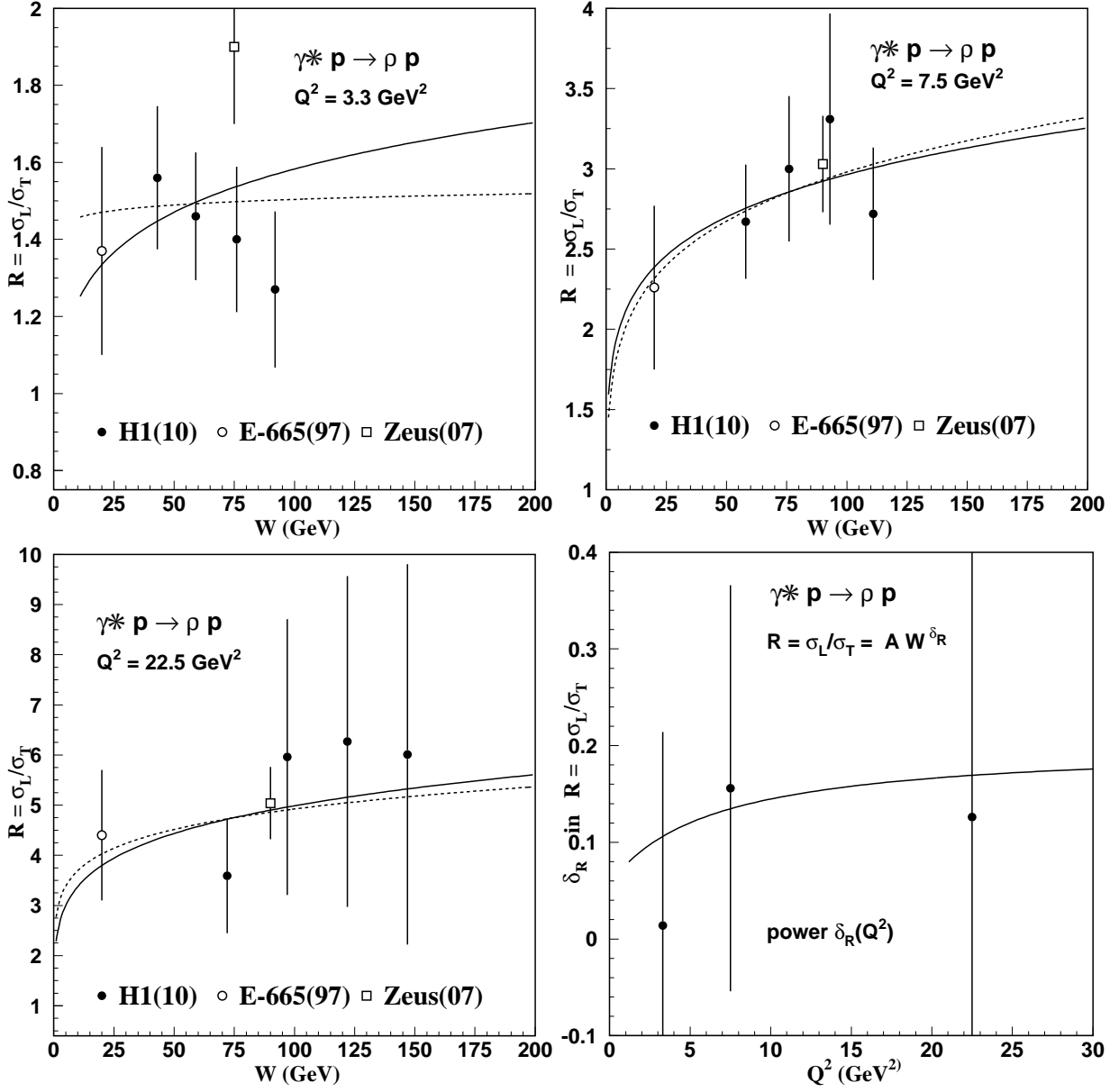
FIG. 8.   a)-c): Energy dependence of the longitudinal to transverse cross section of ρ electroproduction for $Q^2 = 3.3, 7.5$ and 22.5 GeV^2. The solid lines have the energy dependence predicted according to Eq.(30) with Eq.(23), and the dotted lines are free best fits to the data. The data are from [36, 45, 58] d) Power δ_R for the energy dependence of the ratio as function of Q^2. The solid line is $\delta_L - \delta_T$ from Eq.(23), the points with error bars are from the best fits to the data presented in the plots a)-c).

V. SUMMARY AND CONCLUSIONS

We present a simple phenomenological model assuming that single pomeron exchange determines electromagnetically induced diffractive processes. The main consequence of this approach is that the high energy behaviour of each process is determined by a single power W^η. Recent results for J/ψ photoproduction from LHC [22, 23] indicate such a behaviour, which will be tested with more measurements of diffractive electromagnetic processes at LHC.

We furthermore assume that the intercept is determined by the scale of the reaction , which is related to the extension of the dipole wave functions, as illustrated in Fig. 1. This assumption is inspired by a holographic model which predicts a scale dependence of the pomeron slope [27], and is here extended to a model where also the intercept is scale dependent. This assumption is necessary if one assumes a single pomeron exchange, since in photon-induced electromagnetic diffraction processes the energy behaviour depends strongly on the photon virtuality. The scale for vector meson production is in our approach determined by the extension parameter ζ of light cone wave functions [34] and we determine the scale dependence of the pomeron intercept by the energy dependence of the structure function F_2 at fixed Q^2. We have tested two methods for the extraction of this scale and also two extremely different dipole cross sections, illustrated in Fig. 2. It turns out that the uncertainties induced by the different methods of definition of the scale are smaller than present experimental errors.

The assumption of a universal scale, determined essentially by the effective dipole size of the virtual photon, is well compatible with the present data. Specifically the energy dependences of J/ψ and Υ production are successfully predicted. A decisive test of the additional hypothesis of an intercept dependence on a universal scale will also be possible as data for more reactions in the LHC energy range become available.

Also the concept of a scale dependent slope of the pomeron trajectory [27] is well compatible with the data [36], as shown in Fig. 7. A possible scenario for trajectories for J/ψ and Υ photoproduction together with the conventional soft pomeron trajectory is displayed in Fig. 9. The intercept $\alpha_P(0)$ and the slope for $t < 0$ are fixed by the model, see Eqs.(23), (28). For $t \gg 0$ where glueball states may be on the trajectory, the hadronic confinement scale becomes relevant and there it should coincide with the soft pomeron, that is the pomeron trajectory relevant for hadronic scattering.

The model is inspired by AdS/CFT type models which yield a scale dependent slope of the pomeron trajectory and, in a typical bottom-up approach, it is based on the phenomenological input of a scale dependent intercept. A real challenge would be to show, at least qualitatively, how a scale dependent intercept can emerge from more fundamental principles.
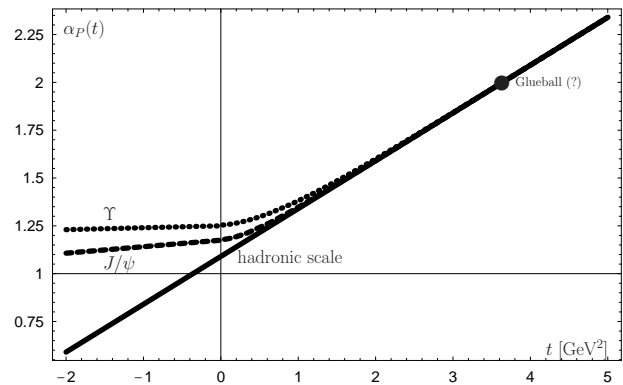

FIG. 9. Scenario for scale dependent pomeron trajectories: the solid line is the trajectory relevant at hadronic scales (soft pomeron), and the dashed and dotted lines represent the trajectories for J/ψ and and Υ photoproduction, respectively.

ACKNOWLEDGMENTS

[1] V. N. Gribov and L. N. Lipatov, Sov. J. Nucl. Phys. **15**, 438 (1972) [Yad. Fiz. **15** (1972) 781]

[2] G. Altarelli and G. Parisi, Nucl. Phys. B **126**, 298 (1977)

[3] Y. L. Dokshitzer, Sov. Phys. JETP **46**, 641 (1977) [Zh. Eksp. Teor. Fiz. **73**, 1216 (1977)]

[4] A. Donnachie and P. V. Landshoff, Phys. Lett. B **296**, 227 (1992)

[5] N. Nikolaev and B. G. Zakharov, Z. Phys. C **53**, 331 (1992)

[6] C. Ewerz and O. Nachtmann, Annals Phys. **322** 1635, 1670 (2007) [hep-ph/0604087].

[7] C. Ewerz, A. von Manteuffel and O. Nachtmann, Phys. Rev. D **77** (2008) 074022 [arXiv:0708.3455 [hep-ph]].

[8] V. S. Fadin, E. A. Kuraev and L. N. Lipatov, Phys. Lett. B **60**, 50 (1975)

[9] E. A. Kuraev, L. N. Lipatov and V. S. Fadin, Sov. Phys. JETP **45**, 199 (1977) [Zh. Eksp. Teor. Fiz. **72**, 377 (1977)]

[10] I. I. Balitsky and L. N. Lipatov, Sov. J. Nucl. Phys. **28** 822 (1978) [Yad. Fiz. **28**, 1597 (1978)]

[11] M. Ciafaloni and G. Camici, Phys. Lett. B **430**, 349 (1998) [hep-ph/9803389].

[12] V. S. Fadin and L. N. Lipatov, Phys. Lett. B **429**, 127 (1998) , [hep-ph/9802290].

[13] A. Donnachie and P. V. Landshoff, Phys. Lett. B **437**, 408 (1998)

[14] H. G. Dosch, E. Ferreira and A. Kramer, Phys. Rev. D **50**, 1992 (1994) [hep-ph/9405237].

[15] H. G. Dosch, T. Gousset and H. J. Pirner, Phys. Rev. D **57** 1666 (1998) [hep-ph/9707264].

[16] G. Kulzinger, H. G. Dosch and H. J. Pirner, Eur. Phys. J. C **7**, 73 (1999) [hep-ph/9806352]

[17] A. Donnachie, H. G. Dosch and M. Rueter, Eur. Phys. J. C **13**, 141 (2000)

[18] A. Donnachie and H. G. Dosch, Phys. Lett. B **502**, 74 (2001) ; Phys. Rev. D **65**, 014019 (2002)

[19] H. G. Dosch and E. Ferreira, Eur. Phys. J. C **29**, 45 (2003)

[20] H. G. Dosch and E. Ferreira, Eur. Phys. J. C **51**, 83 (2007)

[21] V. L. Baltar, H. G. Dosch and E. Ferreira, Int. J. Mod. Phys. A **26**, 2125 (2011)

[22] R. Aaij et al. [LHCb Coll.], J. Phys. G **41** , 055002 (2014)

[23] B. Abelev et al. [Alice Coll.], Phys. Rev. Lett. **113**, 232504 (2014)

[24] J. M. Maldacena, Int. J. Theor. Phys. **38**, 1113 (1999)

[25] S. S. Gubser, I. R. Klebanov and A. M. Polyakov, Phys. Lett. B **428**, 105 (1998)

[26] E. Witten, "Anti-de Sitter space and holography," Adv. Theor. Math. Phys. **2**, 253 (1998)

[27] R. C. Brower, J. Polchinski, M. J. Strassler and C. I. Tan, JHEP **0712**, 005 (2007)

[28] Y. Hatta, E. Iancu and A. H. Mueller, JHEP **0801**, 026 (2008) [arXiv:0710.2148 [hep-th]].

[29] A much more elaborated version of this simple model is given in [27], but the simple form seems to be a god starting point for a phenomenological bottom-up approach

[30] S. J. Brodsky and G. F. de Teramond, Phys. Rev. Lett. **96** (2006) 201601 [hep-ph/0602252].

[31] G. F. de Teramond and S. J. Brodsky, Phys. Rev. Lett. **102**, 081601 (2009)

[32] S. J. Brodsky, G. F. de Teramond, H. G. Dosch and J. Erlich, arXiv:1407.8131 [hep-ph] ; Phys. Rep. C , to appear.

[33] J. Forshaw and R. Sandapen, PoS DIS **2013**, 089 (2013) [arXiv:1305.3768 [hep-ph]]

[34] G.P. Lepage and S.J. Brodsky, Phys. Rev. D **22**, 2157 (1980)

[35] V. Radescu [H1 and ZEUS Coll.], Conf. Proceedings, arXiv:1308.0374 [hep-ex] (2013)

[36] F. D. Aaron et al., JHEP 1005, 032 (2010); [arxiv:0910.5831]

[37] F. J. Gilman, J. Pumplin, A. Schwimmer and L. Stodolsky, Phys. Lett. B **31** 387 (1970) .

[38] Y. S. Jeong, C. S. Kim, M. V. Luu and M. H. Reno, JHEP **1411** , 025 (2014) [arXiv:1403.2551 [hep-ph]].

[39] C. Ewerz, A. von Manteuffel and O. Nachtmann, JHEP **1103**, 062 (2011) [arXiv:1101.0288 [hep-ph]].

[40] K. A. Olive *et al.* [Particle Data Group Coll.], Chin. Phys. C **38** 090001 (2014)

[41] C. Adloff et al. [H1 Coll.], Phys. Lett. B **520** , 183 (2001)

[42] S. Chekanov et al. [Zeus Coll.], Phys. Lett. B **697**, 184 (2011)

[43] J.Breitweg et al., Eur. Phys. J. C **2**, 247 (1998)

[44] M. Derrick et al., Eur. Phys. J. C **6**, 603 (1999)

[45] S. Chekanov , PMC Physics A 1:6 (2007)

[46] C. Adloff et al., Eur. Phys. J. C **13**, 371 (2000)

[47] S. Chekanov et al. Nucl.Phys B **718** , 3 (2005)

[48] A. Aktas et al., , Eur. Phys. J. C **46**, 585 (2006)

[49] C. Alexa et al. , Eur. Phys. J. C **73** , 2466 (2013)

[50] S. Chekanov et al. , Eur. Phys. J. C **24**, 345 (2002)

[51] S. Chekanov et al. , Nucl. Phys. B **695**, 3 (2004)

[52] S. Chekanov et al. , Phys. Lett. B **680**, 4 (2009)

[53] R.M. Egloff, P.J.Davis, G.J.Luste, J.F.Martin and J.D.Prentice , Phys. Rev. Lett. **43** , 657 (1979)

[54] J.J. Aubert et al. [EMC Coll.] , Phys. Lett B **161**, 203 (1985) ; J. Ashman et al. [EMC Coll.] , Zeit.Phys. C **39**, 169 (1988)

[55] S. Aid et al., [H1 Coll.], Nucl.Phys. B **463** 3 (1996)

[56] B.H. Denby et al., Phys. Rev. Lett. **52** , 795 (1984) ; M.E. Binkley et al., Phys. Rev. Lett. **48**, 73 (1982)

[57] C. Alexa et al. [H1 Coll.], Eur. Phys. J. C **73** , 2466 (2013)

[58] M. R. Adams et al., Zeit. Phys. C 74 , 237 (1997)